Zinc-sensitive MRI contrast agents: importance of local probe accumulation in zinc-rich tissues

Kyangwi Malikidogo, Manon Isaac, Adrien Uguen, Sandra Même, Agnès Pallier, Rudy Clémençon, Jean-François Morfin, Sara Lacerda, Éva Tóth, Célia Bonnet

COMMUNICATION

Zinc-Sensitive MRI Contrast Agents: Importance of Local Probe Accumulation in Zinc-Rich Tissues

Accepted 00th January 20xx

DOI: 10.1039/x0xx00000x

Kyangwi P. Malikidogo,[a] Manon Isaac,[a] Adrien Uguen,[a] Sandra Même,[a] Agnès Pallier,[a] Rudy Clémençon, Jean-François Morfin,[a] Sara Lacerda,[a] Éva Tóth,[a] and Célia S. Bonnet*[a]

We present the in vitro characterisation of a Gd^{3+}-based contrast agent that responds to Zn^{2+} upon interaction with Human Serum Albumin. We show that the contradictory in vivo behaviour is related to Gd^{3+}-accumulation in Zn-rich tissues. This highlights the importance of the biodistribution of such contrast agents.

Zinc is a transition metal ion that plays important roles in both healthy and pathological processes. Its misregulation has been connected to cancers,[1] neurodegenerative conditions[2] or diabetes.[3] Many fluorescent sensors have been developed to detect Zn^{2+} *in vitro* and *in vivo*.[4] *In vivo*, low light penetration limits their use to surface imaging. Magnetic Resonance Imaging (MRI) gives complementary information as it has no depth limitation, and provides high resolution for whole body imaging. The sensitivity of MRI is rather low; however, the micro- to millimolar Zn^{2+} concentration in organs such as the pancreas and the prostate[5] renders it perfectly detectable. Recent years have witnessed important development in Zn^{2+}-responsive MRI contrast agents, mainly based on Gd^{3+}.[6] Following the first detection, a decade ago, of Zn^{2+}-release from pancreatic β-cells upon glucose stimulation,[7] spectacular progress has been made in *in vivo* imaging, pioneered by the group of D. Sherry.[8] For example, new insights were gained into the role of Zn^{2+} in endocrine glucose metabolism,[9] and differences in Zn^{2+} release could be detected depending on the physiological/pathological state of the prostate after glucose stimulation.[10]

Most of these studies were performed using a Gd^{3+}-based contrast agent that responds to Zn^{2+} in the presence of Human Serum Albumin (HSA), the most abundant blood protein. The relaxivity response of this type of agents to Zn^{2+} reaches its maximum at 20-80 MHz, and is related to a change in their rotational motion upon HSA binding. However, most imaging studies are performed at higher field (typically 9.4 T), where MRI sensitivity is better, but the relaxivity response based on variation of the rotational dynamics vanishes. For example, the most successful contrast agent used *in vivo* shows 200% relaxivity increase upon Zn^{2+} binding at 0.5 T, *in vitro* and in the presence of HSA, but the relaxivity increase drops to 8 % at 9.4 T[11] where the *in vivo* studies were performed.

Even if insights into the interaction between Zn^{2+}, the contrast agent and HSA have been obtained *in vitro,*[11] better understanding of the molecular bases driving the MRI response to Zn^{2+} in the much more complex *in vivo* environment remains an important challenge. Such information is primordial both for the rational design of optimised high-field Zn^{2+} responsive MRI probes and for the interpretation of *in vivo* data. This could ultimately shed new light on the biology of Zn^{2+}.

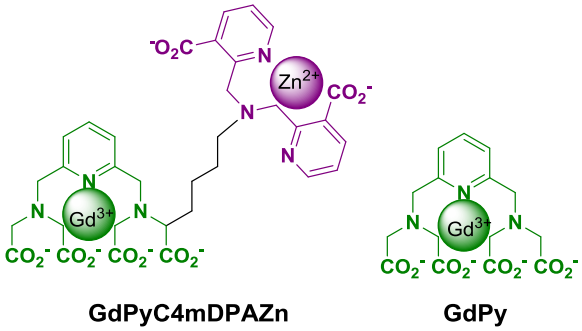

Scheme 1. Chemical structures of the complexes discussed in this work. The green part of the ligand binds Gd^{3+} and the violet part (DPA derivative) is the Zn^{2+}-binding moiety.

In this context, the specific objective of our study was to discriminate two effects potentially leading to an *in vivo* MRI response to Zn^{2+}: (i) the Zn^{2+}-dependent relaxivity increase of the probe, and (ii) its local accumulation in an environment that is rich in Zn^{2+} vs. another tissue, poor in Zn^{2+}. Towards this aim, we have selected GdPyC4mDPA (Scheme 1) which exemplifies the class of Zn^{2+}-responsive MRI probes relying on ZnDPA-HSA interactions and which was previously used in an *in vitro* proof-of-concept study of bimodal Zn^{2+} quantification.[12] First, we show that the combination of good thermodynamic stability and kinetic inertness makes this acyclic, bishydrated complex adapted for preclinical *in vivo* MRI. The particularity of GdPyC4mDPA is that it has a small negative relaxivity change upon Zn^{2+} binding at 9.4 T (*ca.* 8 % r_1 decrease) which enables direct discrimination between a relaxivity response (leading to MR intensity decrease) and local agent accumulation (leading to MR intensity increase). Using *ex vivo* ICP quantification of Zn and Gd contents in tissues, we

could relate the *in vivo* MR signal enhancement observed in the presence of Zn^{2+} to local GdPyC4mDPA accumulation in the Zn^{2+}-rich pancreas. This constitutes the first direct evidence of the role of probe accumulation in explaining the MRI findings when using such Zn^{2+}-responsive MRI contrast agents.

PyC4mDPA was synthesized in 6 steps as previously reported.[12] The good thermodynamic stability of its Gd^{3+} complex (log K = 20.1) was further confirmed by pH dependent relaxivities for GdPyC4mDPA (Figure S1) and luminescence data for the corresponding EuPyC4mDPA (Figure S2). We note that at physiological pH, GdPyC4mDPA is protonated on the DPA amine (log K_H = 8.92).[12] The kinetic inertness of Gd^{3+} complexes is often assessed in transmetalation assays using Zn^{2+} or Cu^{2+} as competing metal ions. Here Zn^{2+} cannot be used as the thermodynamic stability constant of ZnPyC4mDPA (log K_{ZnL} = 16.5)[12] is four orders of magnitude lower than that of GdPyC4mDPA. For GdDTPA, which has also higher stability than ZnDTPA, the displacement of Gd^{3+} by Zn^{2+} is possible due to the formation of a dinuclear Zn^{2+} complex;[13] however, such Zn_2L complex was not observed for the parent GdPy complex.[14] Moreover, in GdPyC4mDPA, the Zn-binding DPA moiety will bind both Zn^{2+} and Cu^{2+}. Water proton T_2 measurements show that even in hard conditions such as 40 eq. of Cu^{2+} at pH 3.5, only 60 % of Gd^{3+} is released (Figure S3) evidencing that Cu^{2+} does not efficiently displace Gd^{3+}. Therefore, the kinetic inertness of GdPyC4mDPA was investigated in Eu^{3+} transmetalation experiments (10-40 fold Eu^{3+} excess to ensure pseudo-first-order conditions). Dissociation was monitored by luminescence in the pH range 3.55-5.03 (Figure 1). The observed rate constants, k_{obs}, show second order dependence on proton concentration, and can be fitted to $k_{obs} = k_0 + k_1[H^+] + k_2[H^+]^2$. k_0 was fixed to zero, otherwise a small value was obtained with large error ($(2.7\pm8.3)\times10^{-5}$). The constants k_1 and k_2 (Table S1) are similar for GdPyC4mDPA and GdPy, evidencing a negligible effect of the Zn^{2+} chelating moiety on the Gd^{3+} dissociation.

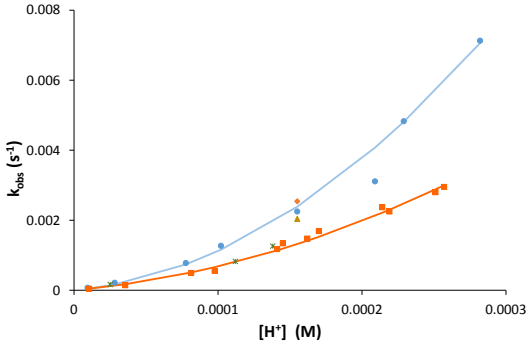

Fig. 1. Observed dissociation rate constants, k_{obs}, as a function of proton concentration for the dissociation of GdPyC4mDPA (100 µM; ●) and GdPy (145 µM, ■) in the presence of 10 eq. of Eu^{3+}; GdPyC4mDPA (100 µM) with 20 eq. (◆), or 30 eq. (▲), or 40 eq. (*) of Eu^{3+} at 25 °C in the presence of 0.1 M NaCl.

The rate constant k_1 (3.6 $mol^{-1}.L.s^{-1}$), characterizing the proton assisted dissociation is nearly one order of magnitude higher than that for GdDTPA (0.58 $mol^{-1}.L.s^{-1}$), while k_2 (7.60×10^4 $mol^{-2}.L^2.s^{-1}$) is in the same order (9.7×10^4 $mol^{-2}.L^2.s^{-1}$).[13] The dissociation half-lives extrapolated to pH 7 exceed 1300 h for both bishydrated complexes GdPyC4mDPA and GdPy, which is more than six times than that for GdDTPA (202 h). This is related to the rigid ligand skeleton which makes difficult structural rearrangements required for dissociation, as previously observed for another pyridine-based Gd^{3+} chelate.[15] GdPyC4mDPA has therefore similar stability and inertness features as the parent compound GdPy whose non-toxicity has been previously evidenced in mice.[16]

Upon Zn^{2+} addition to GdPyC4mDPA, a significant relaxivity change is observed exclusively when Human Serum Albumin is also present.[12] HSA possesses several binding sites, including two hydrophobic pockets (site I and II), and four metal binding sites. Two of them show significant affinity for Zn^{2+} of 100 nM[17] and 2 µM.[18] We have previously shown that GdPyC4mDPA interacts with HSA through at least five binding sites, whether Zn^{2+} is present or not. Some of these interactions are probably non-specific. In order to characterize binding to specific site II, competitive fluorescence measurements were performed using Dansylglycine as a competitor (Figure S5, Table 1). The affinity of GdPyC4mDPA for site II is doubled in the presence of Zn^{2+}, and this is confirmed by K_D values calculated from relaxometric titrations (Figure S6). The affinity found in the presence of Zn^{2+} is also consistent with data for another DPA-containing ligand, despite the charge difference.[19] Importantly, these results evidence that the protein-bound fraction of GdPyC4mDPA will be more important in Zn-rich tissues.

Table 1. Conditional dissociation constants (K_D) measured by paramagnetic relaxation enhancement (PRE) and fluorescence competition experiments using Dansylglycine in site II, at 37 °C and pH 7.4.[a]

K_D (µM)	PRE	Fluorescence
GdPyC4mDPA	60 ± 20	45 ± 10
GdPyC4mDPAZn	30 ± 10	25 ± 10

[a] A K_D of 3.4 µM for Dansylglycine for the site II of HSA was used for the fitting (see Figure S4).

Next, the relaxometric properties of GdPyC4mDPA have been assessed in detail. The fit of the ^1H NMRD (Nuclear Magnetic Relaxation Dispersion) profiles (Figure S7) using the Solomon-Bloembergen-Morgan (SBM) theory yields a rotational correlation time (185 ps) which is consistent with the molecular size (see Table S2 for all parameters). This NMRD profile is not modified significantly in the presence of Zn^{2+} (Figure S8). Figure 2 compares the NMRD profiles of GdPyC4mDPA in the presence of physiological concentration of HSA with and without 1 eq. of Zn^{2+}. The hump at ~80 MHz confirms slow rotation, thus interaction of the complex with HSA, both with and without Zn^{2+}. Under the conditions used, >90% of GdPyC4mDPA is bound to HSA, whether Zn^{2+} is present or not. Therefore, the NMRD profiles are characteristic of the bound species, within experimental error. Luminescence lifetime measurements on the Eu^{3+} analogue prove that the hydration number of Gd^{3+} does not significantly change in the presence of HSA, whether Zn^{2+} is present or not (q = 2; Table S3). The profiles were analysed with the SBM theory including

the Lipari Szabo approach (equations in ESI), which takes into account a local motion of the Gd^{3+} complex (τ_l^{298}) and a global motion of the protein (τ_g^{298}).

Again, the parameters characterizing rotational dynamics in the presence of HSA, without or with Zn^{2+}, are the most relevant (Table 2 and S4). In particular, S^2 reflects the degree of spatial restriction of the local with respect to the global motion, and its ~50% increase upon Zn^{2+} binding points to a more pronounced rigidity. It indicates that the relaxivity increase observed at medium fields in the presence of Zn^{2+} (in 0.6 mM HSA) can be ascribed to an increased rigidity of the ternary GdPyC4mDPA-Zn-HSA complex with respect to GdPyC4mDPA-HSA.

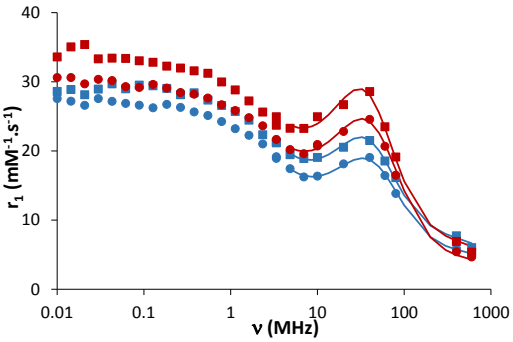

Fig. 2. ^{1}H NMRD profile of GdPyC4mDPA (Blue) and GdPyC4mDPAZn (Red) at 0.3 mM, 25 °C (■), and 37 °C (●) in the presence of 0.6 mM of HSA at pH 7.4 (HEPES 0.1 M). The lines represent the best fit to the SBM theory using the Lipari-Szabo approach with the parameters in Table 2.

Table 2. Rotational parameters of the complexes in the presence of 0.6 mM of HSA obtained from the fitting of the NMRD profiles to he SBM theory using the Lipari-Szabo approach.

	GdPyC4mDPA	GdPyC4mDPAZn
τ_g^{298} (ps)	2800 ± 200	2900 ± 200
τ_l^{298} (ps)	112 ± 4	110 ± 9
S^2	0.14 (1)	0.21 (1)

Upon Zn^{2+} binding, GdPyC4mDPA shows a modest relaxivity increase (*ca.* 30 %) at 0.94 T (40 MHz), while at 9.4 T (400 MHz) the relaxivity decreases by *ca.* 8%. This small relaxivity decrease is reflected by the phantom images in mouse serum (Figure 3), but would be likely insufficient for *in vivo* zinc detection. On the other hand, given the enhanced HSA affinity of GdPyC4mDPA in the presence of Zn^{2+}, we hypothesized that local accumulation of the probe in Zn^{2+}-rich tissues could compensate for the lack of relaxivity increase. To test this hypothesis, we monitored Zn^{2+} release from the pancreas after glucose injection in mice by MRI, following GdPyC4mDPA administration.

Pancreas has a particularly high Zn^{2+} content (µM to mM). Zn^{2+} ions are necessary for proper insulin storage in granules in β-cells.[1] Injection of a glucose bolus stimulates co-release of insulin and Zn^{2+} from β-cells into the extracellular media, rendering it amenable for MRI detection. Such protocol was successfully applied to Zn^{2+} detection by MRI, using a Zn^{2+}-responsive contrast agent that showed significant relaxivity increase upon Zn^{2+} binding both at 23 MHz and 400 MHz.[7]

Fig 3. T_1-weighted phantom images in mouse serum without or with 0.2 mM GdPyC4mDPA in the presence and in the absence of 1 eq. of Zn^{2+} (37 °C). Images were acquired at 9.4 T using spin echo sequence with TE = 16 ms, TR = 500 ms.

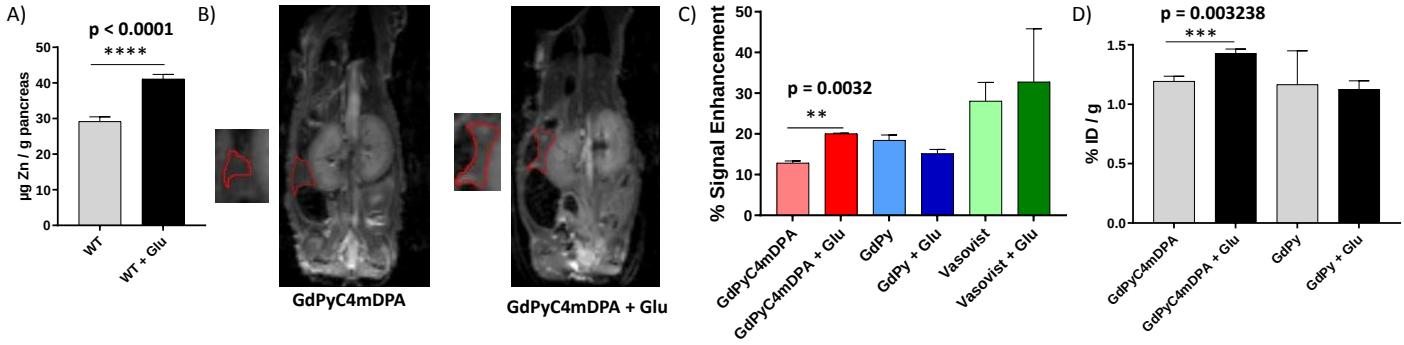

Fig. 4. A) Zn content in the pancreas measured by ICP-OES for mice with and without glucose injection. Animals were euthanized 20 min after glucose injection, and pancreas were excised and digested in HNO_3 prior to analysis; data are presented in µg Zn per g of pancreas (n = 6, ±SEM; p < 0.0001); B) T1-weighted MR images of mouse pancreas (outlined in red) 10 min post i.v. injection of **GdPyC4mDPA** without and with glucose injection (10 min prior to **GdPyC4mDPA** injection); C) % of MRI signal enhancement in the pancreas after i.v. injection of 44 µmol.kg^{-1} of **GdPyC4mDPA**, **GdPy** or **Vasovist**® without and with glucose injection 10 min prior to contrast agent injection (n = 3, ±SEM; p = 0.0032); D) Gd content in the pancreas measured by ICP-OES for mice with and without glucose injection. Animals were euthanized 10 min after contrast agent injection, and pancreas were excised and digested in HNO_3 prior to analysis; data are presented in % of injected dose by organ mass (n = 3, ±SEM; p = 0.0138).

Mice were divided into two groups: the WT+Glu group received an intraperitoneal bolus of 20% glucose 10 min prior to intravenous contrast agent injection (44 µmol.kg^{-1}), while the control group (WT) received only the contrast agent. To confirm the pertinence of the model, Zn^{2+} content was measured *ex vivo* by Inductively Coupled Plasma Optical Emission Spectroscopy (ICP-OES) in various organs for the two groups 20 min and 70 min after glucose injection (Figure 4A and S9). At 20 min, 40% higher zinc content was found in the pancreas for the group which received glucose injection, while there was no significant change in the zinc level at 20 min in other organs, nor at 70 min in any organ. All data are consistent with literature values.[20] These results confirm the significant glucose-dependent difference in Zn^{2+} level of the pancreas. Mice were imaged by MRI at 9.4 T after injection of 44 µmol.kg^{-1} of GdPyC4mDPA, GdPy or Vasovist®, a blood-pool agent which binds to HSA (Figures 4 and S10). 10 min after GdPyC4mDPA injection, significantly higher MRI intensity is observed in the pancreas of mice in the Glu group versus control (WT group, no glucose) animals (Figure 4B and C). In all other organs, MRI intensities are similar for the two groups over the time course of the experiment (Figure S10). For GdPy and Vasovist®, no MRI intensity differences are observed between the two groups, either in the pancreas or in any other organ, highlighting the importance of the presence of the "Zn^{2+} binding unit" in GdPyC4mDPA, leading to a zinc-dependent tissue accumulation, which will in turn lead to the increased MRI signal intensity. As the change in GdPyC4mDPA relaxivity upon Zn^{2+} binding cannot explain the MRI response observed, an *ex vivo* biodistribution was performed by ICP-OES, in similar conditions. Gadolinium contents were measured 10 min and 1h post contrast agent injection in the pancreas and other organs of interest (Figures 4D and S11). In the case of GdPyC4mDPA, the Gd content of the pancreas is 20% higher in the Glu group compared to the control group. No significant differences are detected in other organs, nor upon injection of GdPy. For the first time, these data unambiguously show that the MRI response observed in the pancreas after glucose injection is not the result of a relaxivity change, but the consequence of local accumulation of GdPyC4mDPA, promoted by an elevated Zn^{2+} level. This is certainly due to the doubled HSA affinity of GdPyC4mDPA in the presence of Zn^{2+}, resulting in a longer circulation time and better accumulation of the contrast agent in Zn-rich tissues. This information is crucial to understand the *in vivo* behaviour of such Zn^{2+} responsive probes and to improve their MRI response.

To conclude, GdPyC4mDPA provides sufficient thermodynamic stability and kinetic inertness for preclinical use. The dissociation half-life of the bishydrated, open-chain Gd^{3+} complex estimated for physiological pH is six times higher than that for GdDTPA, and related to the high rigidity of the Gd^{3+}-chelating moiety. GdPyC4mDPA binds HSA and its binding affinity doubles in the presence of Zn^{2+}. The increased rigidity of the ternary GdPyC4mDPA-Zn-HSA complex formed upon Zn^{2+} binding leads to slightly increased relaxivity at intermediate fields and a small relaxivity decrease at high field (9.4 T). In sharp contrast, *in vivo* experiments in mice evidence MR signal intensity increase in the pancreas upon glucose stimulation and concomitant Zn^{2+} release. Based on *ex vivo* ICP-OES data, we can unambiguously relate this to local GdPyC4mDPA accumulation in tissues rich in Zn^{2+}. This underlines that for such protein-bound Zn^{2+} responsive probes, the *in vivo* MRI response is strongly guided by the different probe biodistribution between tissues rich or poor in Zn^{2+}, while relaxivity variations can be negligible. To the best of our knowledge, this is the first time that such accumulation effect is highlighted. We believe that this important finding will help understand the *in vivo* behaviour of such systems and contribute to the development of Zn^{2+} responsive probes for high field MRI detection. Indeed, the chemical design of contrast agents that respond to Zn^{2+} in the presence of HSA should seek primarily for highly Zn^{2+}-dependent HSA binding affinities.

We thank Drs Alkystis Phinikaridou and René M. Botnar for providing Vasovist®, and Dr Frederic Szeremeta for his help in

in vivo experiments. We acknowledge the support from ITMO Cancer of Aviesan within the framework of 2021-2030 cancer control strategy on funds administered by Inserm and La Ligue Contre le Cancer (grants PM-FP/2021-407 and PM-FP/2020-244). MA thanks the European Union's Horizon 2020 research and innovation program under the Marie Sklodowska-Curie grant agreement No 898850.

Conflicts of interest

There are no conflicts to declare.

Notes and references

1. S. L. Kelleher, N. H. McCormick, V. Velasquez and V. Lopez, *Adv. Nutr.*, 2011, **2**, 101-111.
2. P. Faller and C. Hureau, *Chem. Eur. J.*, 2012, **18**, 15910-15920.
3. S. A. Myers, *Int. J. Endocrinol.*, 2015, **2015**, 167503-167503.
4. Y. Chen, Y. Bai, Z. Han, W. He and Z. Guo, *Chem. Soc. Rev.*, 2015, **44**, 4517-4546.
5. L. De Leon-Rodriguez, A. J. M. Lubag and A. D. Sherry, *Inorg. Chim. Acta*, 2012, **393**, 12-23.
6. C. S. Bonnet, *Coord. Chem. Rev.*, 2018, **369**, 91-104.
7. A. J. M. Lubag, L. M. De Leon-Rodriguez, S. C. Burgess and A. D. Sherry, *PNAS*, 2011, **108**, 18400-18405.
8. P. Khalighinejad, D. Parrott and A. D. Sherry, *Pharmaceuticals*, 2020, **13**, 268.
9. V. C. Jordan, C. D. G. Hines, L. T. Gantert, S. B. Wang, S. Conarello, C. Preihs, S. Chirayil, M. Klimas, J. L. Evelhoch and A. D. Sherry, *Frontiers in Endocrinology*, 2021, **12**.
10. M. V. C. Jordan, S.-T. Lo, S. Chen, C. Preihs, S. Chirayil, S. Zhang, P. Kapur, W.-H. Li, L. M. De Leon-Rodriguez, A. J. M. Lubag, N. M. Rofsky and A. D. Sherry, *PNAS*, 2016, **113**, E5464-E5471.
11. A. F. Martins, V. C. Jordan, F. Bochner, S. Chirayil, N. Paranawithana, S. Zhang, S.-T. Lo, X. Wen, P. Zhao, M. Neeman and A. D. Sherry, *J. Am. Chem. Soc.*, 2018, **140**, 17456-17464.
12. K. P. Malikidogo, I. Da Silva, J.-F. Morfin, S. Lacerda, L. Barantin, T. Sauvage, J. Sobilo, S. Lerondel, É. Tóth and C. S. Bonnet, *Chem. Commun.*, 2018, **54**, 7597-7600.
13. L. Sarka, L. Burai and E. Brucher, *Chem. Eur. J.*, 2000, **6**, 719-724.
14. L. Pellegatti, J. Zhang, B. Drahos, S. Villette, F. Suzenet, G. Guillaumet, S. Petoud and E. Toth, *Chem. Commun.*, 2008, 6591-6593.
15. C. S. Bonnet, S. Laine, F. Buron, G. Tircso, A. Pallier, L. Helm, F. Suzenet and E. Toth, *Inorg. Chem.*, 2015, **54**, 5991-6003.
16. C. S. Bonnet, F. Buron, F. Caille, C. M. Shade, B. Drahos, L. Pellegatti, J. Zhang, S. Villette, L. Helm, C. Pichon, F. Suzenet, S. Petoud and E. Toth, *Chem. Eur. J.*, 2012, **18**, 1419-1431.
17. W. Bal, M. Sokolowska, E. Kurowska and P. Faller, *Biochimica Et Biophysica Acta-General Subjects*, 2013, **1830**, 5444-5455.
18. C. André and Y. C. Guillaume, *Talanta*, 2004, **63**, 503-508.
19. A. C. Esqueda, J. A. Lopez, G. Andreu-De-Riquer, J. C. Alvarado-Monzon, J. Ratnakar, A. J. M. Lubag, A. D. Sherry and L. M. De Leon-Rodriguez, *J. Am. Chem. Soc.*, 2009, **131**, 11387-11391.
20. Y. A. Seo, J. A. Elkhader and M. Wessling-Resnick, *BioMetals*, 2016, **29**, 147-155.